Phenomenology of Doppler forward scatter radar for surface targets observation

Gashinova, Marina; Daniel, Liam; Hoare, Edward; Sizov, Vladimir; Cherniakov, Mikhail

DOI:
10.1049/iet-rsn.2012.0233

Document Version
Publisher's PDF, also known as Version of record

Citation for published version (Harvard):
Gashinova, M, Daniel, L, Hoare, E, Sizov, V & Cherniakov, M 2013, 'Phenomenology of Doppler forward scatter radar for surface targets observation', *IET Radar, Sonar and Navigation*, vol. 7, no. 4, pp. 422.
https://doi.org/10.1049/iet-rsn.2012.0233

www.ietdl.org

Published in IET Radar, Sonar and Navigation
Received on 16th August 2012
Revised on 26th October 2012
Accepted on 12th November 2012
doi: 10.1049/iet-rsn.2012.0233

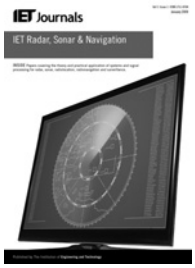

ISSN 1751-8784

Phenomenology of Doppler forward scatter radar for surface targets observation

Marina Gashinova[1], Liam Daniel[1], Vladimir Sizov[2], Edward Hoare[1], Mikhail Cherniakov[1]

[1]Department of Electronic, Electrical and Computer Engineering, University of Birmingham, Birmingham B15 2TT, UK
[2]Department of Radioelectronics, National Research University of Electronic Technology, Zelenograd, Moscow 124498, Russia
E-mail: m.s.gashinova@bham.ac.uk

Abstract: In this study, the forward scatter Doppler phase signature formation is analysed to show the rationale for the forward scatter radar in the true sense of the meaning, where a target actually crosses the baseline; so the advantage of the main shadow lobe is taken and, therefore a forward scatter effect occurs to enhance signal to clutter ratio. The modelling approach suggested is based on the consideration of the Doppler phase signature as a result of superposition of the direct path signal and the shadow radiation signal. It is shown that the target signature may be represented as a Doppler signature of a point-like target specified by its trajectory and speed, which is modulated according to forward scatter cross-section of an actual extended target specified by its silhouette at each moment of motion. The proposed model may be recommended to provide matched filtering in coherent processing. Finally, the approach is verified experimentally using calibrated targets with conductive and absorbing coating in the controlled environment and maritime targets in the real sea conditions.

1 Introduction

Forward scatter radar (FSR) is historically thought of as the first type of bistatic radar, which has been reported in [1]. FSR could be viewed as subclass of bistatic radar (BR) where the bistatic angle is close to 180° [2–4], the physical operational principle of FSR is however essentially different from that of BR, which is inherently a backscatter radar. One of the major differences is that the target signature is formed as a result of interference between the direct path (or leakage) signal and the scattered signal from the target, rather than correlation of the received waveform and locally generated heterodyne reference in backscatter radars. This difference affects the method of optimal signal processing [5–7]. Fundamentally the Doppler signature of the target depends on the target electrical dimensions, its shape, trajectory parameters and speed. Practically all these parameters are unknown a priory and, therefore in order to achieve optimal signal processing on the reception side, one should know the means of generating the waveform, which replicates the real signal. To predict a signature the correct model should be available based on comprehensive analysis of the forward scattering (FS) phenomena – this constitutes the main subject of the paper. The proposed modelling procedure is based on consideration of the two main mechanisms contributing to Doppler signature formation: first is the chirp-like Doppler waveform formation because of frequency variation caused by the target motion and the second is the envelope pattern related to the target's electrical dimensions and shape. Optimal signal processing in this case provides not only maximisation of the signal to noise ratio for better target detection, but also allows an estimation of the target's trajectory and speed.

Recently a wave of interest has emerged in FSR; firstly this is a consequence of the introduction of 'stealth' targets. These targets have a significantly reduced radar cross-section (RCS) because of their specific shapes and/or coatings which may greatly suppress backscattering, yet their shadows will still render them perfectly 'visible' to FSR. Secondly, interest in FSR has appeared because of the establishment of passive coherent location concepts [8–9] where illuminators of opportunity are used to form a bistatic radar network.

This paper is concerned with the analysis of a class of FSR where the target actually crosses the baseline (true FSR), introducing a perturbation of the direct path signal and producing a Doppler phase signature with a relatively long observation time. Strictly speaking the radar under analysis is a special-purpose radar intended to detect low profile, low-speed targets, which represent a class of 'difficult surface targets' where traditional monostatic radar has limitations.

FSR exploits the so-called forward scattering (FS) effect for enhanced target detection [4, 10, 11], which occurs if the target's electrical size produces scattering in the Mie and optical regions. The FS effect is the strong increase of RCS in the forward direction caused by the co-phase interference of the waves arising from the shadow contour of the scatterer. This results in a field focusing on the line perpendicular to the object aperture in the shadow area. With an increase in frequency the main shadow lobe

narrows and its peak intensity becomes significantly larger than that of the backscattering lobe, with a maximum along the axis of the main shadow lobe, that is, when the transmitter, receiver and target form ~180° bistatic angle [2, 12].

Initially the FS phenomenon was thoroughly studied in optics, where it was predicted by Mie [13], reported to be observed for the Mie scattering region [14] and quantitatively evaluated by the optical theorem for particles [15]. Subsequently, the effect was investigated in studies dedicated to the estimation of bistatic RCS of objects [11] for microwaves and Ufimtsev [16] developed the physical theory of diffraction.

Although the target is in motion, the scattering mechanism undergoes a fundamental change: bistatic scattering (mainly of the reflective nature) when the receiver is outside the target main shadow lobe transforms into purely FS when the target crosses the baseline and the receiver is in the shadow. Signal analysis with a view to find the transition between the two scattering mechanisms will, firstly, provide a valuable insight into responses from so called 'stealth targets' and, secondly, define the margins of applicability for the suggested model where shadow radiation is the prevailing diffraction mechanism. Results of measurements in the controlled environment of an anechoic chamber will be shown for metallic and absorbing targets of the same geometrical cross-section.

The remainder of the paper is structured as follows: initially, the concept of FSR is described. Next analytical formulae for the Doppler frequency shift and target Doppler phase signature along with a simplified forward scatter cross-section model are presented. RCSs estimated according to the presented approach are compared with those simulated in three-dimensional (3D) full-wave software. Then the validity of the suggested models in optical and sub-optical scattering regions is discussed and comparison with experimental results in both the anechoic chamber and the real environment is given. The paper concludes with a summary of the study's research contributions.

2 FSR phenomenology

In a bistatic radar configuration spatially separated Tx and Rx antennas are pointed to the area where the target of interest appears and it is assumed that the baseline distance is comparable with the distances from Tx/Rx to the target [17]. The signal at the input of the receive antenna represents mainly bistatic reflections of the transmitted signal from the interrogated target and only this reradiated signal is required to extract information about the target if the transmit and receive signals are synchronised.

In contrast, in FSR the Rx and Tx antennas are facing each other and there are two signals, which play equally important roles in forming the sensed interference or 'beat' [4] chirp-like signal: the first is the strong direct path signal, or 'leakage', which may be used only for detection, and the second is the much weaker forward scatter signal from the moving target 'modulating' the leakage, which in fact carries information on target trajectory, speed and even size and profile.

Thus, the operational principle of FSR is based on availability of both signals at the input of the receive antenna.

To provide the presence of both leakage and scattered signal the target-radar topology should satisfy far-field conditions for the target and the receive antenna: the size of the target must be significantly smaller than distances to both Tx and Rx and to the radius of the first Fresnel zone. The target represents a source of secondary radiation with respect to primary radiation from Tx according to Huygens–Fresnel principle.

Using Fresnel parameter $S = D^2/(4\lambda)$, where D is a largest effective size of target and λ is a wavelength we will consider the scattering mechanism from a target as a Fraunhofer diffraction (or far-field) at distances larger than S. However when considering the time-varying Doppler signature of a moving target, we should not confuse Fraunhofer diffraction on the individual target with the Fresnel-like diffraction on the effective inverse aperture defined by the whole path of the moving target which is 'seen' by the radar.

Measured signatures of targets with sizes defining different diffraction mechanisms are shown in Fig. 1 for 7.5 GHz carrier and 300 m baseline: (a) Fraunhofer (far-field) diffraction from a small inflatable boat of size 2.9 m × 1 m (length and height above the surface), $\boldsymbol{S} = 60$ m; (b) boundary Fresnel to Fraunhofer, medium size sailing yacht (5 m × 3 m), $S = 160$ m; and (c) Fresnel diffraction from large motor boat (15 m × 4 m), $S = 630$ m.

The measured signals shown are the received signal strength indicator (RSSI) signals, which contain the oscillating Doppler signature on top of a DC level indicating the strength of the direct path signal. In all signatures, the typical Fresnel diffraction behaviour (positive and negative contribution of phases of interfered signals) is visible at least at the edges of the target signal for cases (b) and (c). Obviously all three signals are liable to detection and, moreover, (b) and (c) are not difficult targets because their scattered signals are comparable with the leakage signal. However, only the first signal is suitable for the extraction of target motion parameters. Indeed, its waveform is fully defined by diffraction reflecting specific positions and speed of the target passing through the constructive (in phase) and destructive (out of phase) zones over the path. It should be stressed that in the middle of the two-sided chirp-like signal the signal intensity is the same as the intensity of the incident (direct path) signal, although intuitively there should be a global minimum because of shadowing. This phenomenon is similar to the Poisson phenomenon (Arago spot) known in optics for Fresnel diffraction.

The Arago spot is quite challenging to observe in optics where the very small wavelength imposes the following conditions: (i) target to be small, perfectly symmetrical and having ideal edges, (ii) distances to the source and the illuminated screen to be in the Fresnel zone and (iii) source of light to be point-like. However scaling up the wavelength, we can expect that a pattern similar to Fresnel rings will appear if the target/wavelength ratio and the total range of target movement satisfy the conditions of Fresnel diffraction. Moreover, the much larger scale and the use of the Doppler signature instead of operational carrier frequency signals weakens the strict conditions on symmetry and smooth edges of the target silhouette on the line of sight, so that the Arago–Poisson spot may appear as soon as the target is on the line of sight. Mathematically it is expressed by the presence of the non-zero imaginary part of the FS amplitude $f(\theta = 0)$, which relates to the total scattering

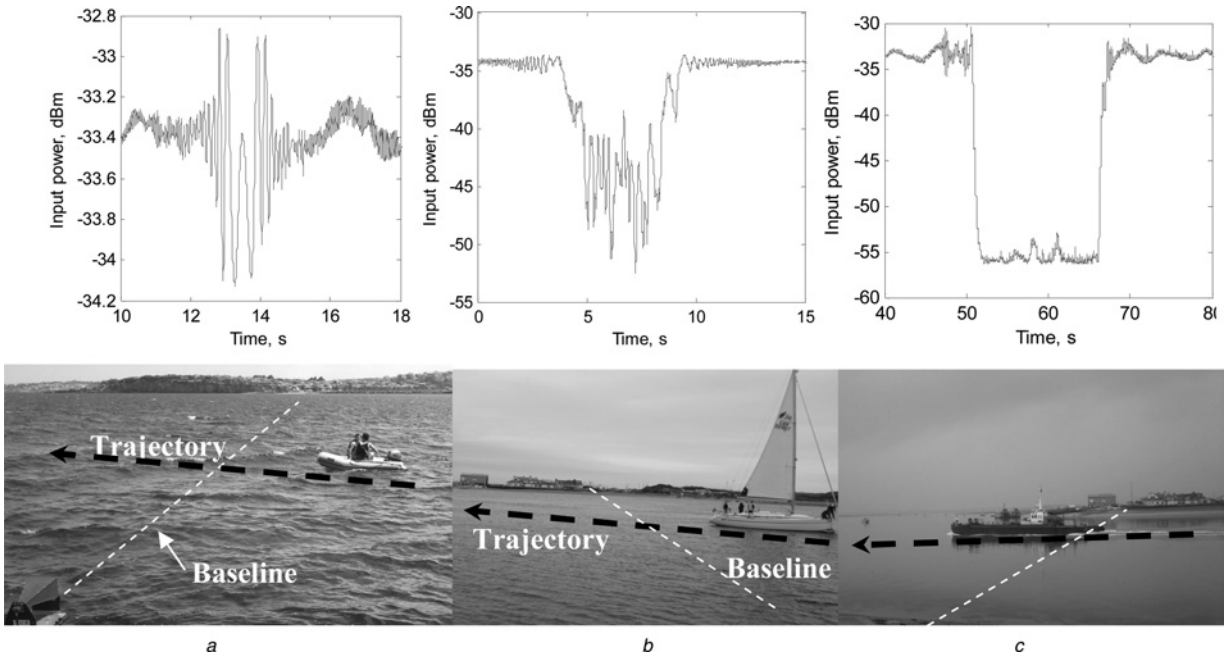

Fig. 1 *Recorded Doppler signature of the targets crossing the centre of 300 m baseline*

a Small inflatable boat
b Medium size yacht
c Large motor boat

cross-section σ_{tot} as

$$\text{Im}\, f(\theta = 0) = \frac{k\sigma_{\text{tot}}}{4\pi} \tag{1}$$

and explained by optical theorem [18, 19].

It should be stressed that the symmetry of the target silhouette to the incident wave is still required for the quasi-optical region; however, it is less strict when we move down in frequency. We can suppose that if the wavelength is nearly comparable to the effective target dimensions its asymmetry will be not resolved by the incident and diffracted waves.

When the target moves, sequentially passing constructive and destructive zones, the time domain waveform of the Doppler signature develops in time in the same manner as the Fresnel rings progress in space. The larger electrically the target the less observable is the Arago spot and the larger the intensity of shadow radiation.

3 Target signature in FSR

3.1 Doppler signature

In this paper, we concentrate on the true FS Doppler signature when the target shadows the receiver. Following Ufimtsev [10] the physical idea of the shadowed direct path signal can be understood by considering the field at the receiver as the result of interference of the incident electromagnetic field and the shadow radiation from the scattering body. Hence, the physical optics (PO) approximation will be the right amount of theory to gain insight into the phenomenon. The question of more accurate electromagnetic diffraction is out of the scope of this paper and may be found in [16].

We assume that target has a uniform linear trajectory. This is nearly always true for surface targets: they have a relatively narrow FS CS pattern, consequently visibility time, or signature length, is the order of seconds and it is not likely that they will make a significant manoeuvre or change of speed over this short time.

Shadow radiation is cast upon the receiver while the target moves in the vicinity of the baseline according to the width of the shadow lobe. The maximum of the shadow radiation corresponds to the case when the target is on the baseline. Being 'shadow' the forward scatter signal is $\pi/2$ phase shifted (imaginary along the FS axis) relative to the direct path signal [10, 19].

At this stage we omit any amplitude modulation of the signal caused by propagation loss and by the FS CS pattern. Only the phase signature of the point-like target (yet casting shadow on the receiver) will be initially derived.

Later the total target signature will be presented as the result of superposition of the point target phase signature and complex envelope defined by FS CS of the extended target.

At the receiver input a composition of the direct path signal and delayed scattered signal from the moving target is

$$\begin{aligned} S_{\text{RI}}(t) &= S_{\text{DP}} + S_{\text{TG}} \\ &= A_{\text{DP}} \cos(\omega_0 t) + A_{\text{Tg}} \sin\big(\omega_0 (t + t_{sh})\big) \end{aligned} \tag{2}$$

where ω_0 is the carrier, t_{sh} is the delay time of the signal from moving target, S_{DP} and S_{TG} are direct path signal and scattered target signal, respectively. The initial phase of coherently acquired signals can be omitted without loss of generality.

Owing to the fact that the Doppler signature in FSR fundamentally occupies a very low-frequency band, in the order of few Hz, the only way to detect this signal within the background of the transmitter phase noise is to use self mixing heterodyne, that is, to segregate this signature by mean of non-linear transformation of the input signal. We

doi: 10.1049/iet-rsn.2012.0233

will consider as an example an envelope detector with quadrature characteristic.

After passing the square law detector and low-pass filter in the receiver the input signal transforms into

$$S_{\mathrm{RO}}(t) \overset{\mathrm{SLD}}{\simeq} \left[A_{\mathrm{DP}}\cos(\omega_0 t) + A_{\mathrm{Tg}}\sin\big(\omega_0(t+t_{sh})\big)\right]^2 \overset{\mathrm{LPF}}{\simeq} DC - A_{\mathrm{Sc}}\sin\big(\omega_0 t_{sh}\big)\big|_{t_{sh}=(R(t)+R(t)-L/c)} = DC - A_{\mathrm{Sc}}\sin\left(\frac{2\pi\big(R_{\mathrm{T}}(t)+R_{\mathrm{R}}(t)-L\big)}{\lambda}\right) \quad (3)$$

where $DC = \big(A_{\mathrm{DP}}^2 + A_{\mathrm{Tg}}^2/(2)\big) \overset{A_{\mathrm{Tg}}\ll A_{\mathrm{DP}}}{\simeq} \big(A_{\mathrm{DP}}^2/2\big)$ is the power of the leakage signal, $A_{\mathrm{Sc}} = A_{\mathrm{DP}}A_{\mathrm{Tg}}$ characterises phase signature amplitude, L is a baseline distance, $R_{\mathrm{T}}(t)$ and R_{R}(t) are time-dependant ranges Tx-to target and target-to-Rx accordingly.

In terms of Doppler phase shift

$$S_{\mathrm{RO}}(t) \overset{\mathrm{SLD}}{\simeq} \left[A_{\mathrm{DP}}\cos(\omega_0 t) + A_{\mathrm{Sc}}\sin\big((\omega_0+\omega_{\mathrm{d}})t\big)\right]^2 \overset{\mathrm{LPF}}{\simeq} DC + A_{\mathrm{Sc}}\sin(\omega_{\mathrm{d}}t) \quad (4)$$

where ω_{d} is the Doppler frequency shift of the moving target.

Thus

$$\omega_{\mathrm{d}}t \equiv -\frac{2\pi}{\lambda}\big(R_{\mathrm{T}}(t)+R_{\mathrm{R}}(t)-L\big) + 2\pi n, \quad n\in\mathbb{Z} \quad (5)$$

The last term can be omitted without loss of generality.

Traditionally [3, 20] bistatic Doppler frequency shift is presented as a derivative of the variable phase shift

$$\omega_{\mathrm{d}} = -k\frac{\mathrm{d}\big(R_{\mathrm{T}}(t)+R_{\mathrm{R}}(t)\big)}{\mathrm{d}t} \quad (6)$$

which to a first approximation may be solved considering ω_{d} as a constant in form

$$\omega_{\mathrm{d}}t + C = -k\big(R_{\mathrm{R}}(t)+R_{\mathrm{T}}(t)\big) \quad (7)$$

Setting the origin of the time coordinate system as zero at the moment of crossing the baseline we can find that the integration constant $C = -kL$ using the initial condition $R_{\mathrm{T}}(t)+R_{\mathrm{R}}(t)/_{t=0} = L$.

Finally

$$\omega_{\mathrm{d}} = \frac{-(2\pi/\lambda)\big(R_{\mathrm{R}}(t)+R_{\mathrm{T}}(t)-L\big)}{t}$$

which coincides with the expression obtained (5) for the phase shift with removable singularity $\omega_{\mathrm{d}} = 0$ at $t = 0$

$$\omega_{\mathrm{d}} = -\frac{2\pi}{\lambda}\frac{\big(R_{\mathrm{T}}(t)+R_{\mathrm{R}}(t)-L\big)}{t} \quad (8)$$

Actual Doppler target signature extracted at the receiver has an envelope $A(t)$ defined by both path propagation loss and FS CS

$$S_{\mathrm{r}}(t) = A(t)\sin[\psi(t)] \quad (9)$$

where $\psi(t) = 2\pi/\lambda(T_{\mathrm{T}}(t)+R_{\mathrm{T}}(t)-BL)$ is the phase of the moving point-like target.

3.2 Signature envelope

Analytical solutions for the FS CS are only available for the few convex shapes using physical theory of diffraction (PTD) approaches for optical and sub-optical scattering regions [21–23]. For the Rayleigh region the diffraction mechanism is more sophisticated and correct analytical solutions are only available for the sphere and infinitely long cylinder. Thus either approximated models, such as suggested by PO or PTD [4, 22, 23] or full-wave EM simulation methods [12, 24] must be used for target FS CS estimation. In general without a prior knowledge of the target shape it is only the phase target signature which can be used for information extraction on target motion. Yet its envelope defined by FS CS as function of time while the target is moving in a specific bistatic configuration indicates the size and shape of the target and enables rough classification based on comparison with the database of known targets [25].

In optical approximation for estimation of the target RCS at FS direction the Babinet principle is used. A flat absorbing screen of finite dimensions may be replaced by a complementary infinite plane screen with an aperture shaped exactly like the original screen. The incident field diffracted at the aperture gives rise to the field coinciding with the shadow field of the original absorbing screen (except for the phase). If the incident wave is a plane wave, as assumed by the target being in the Fraunhofer zone, then the shadow field of a target at a distant receiving point tends to be the radiation field of a flat aperture placed perpendicular to the incident wave propagation direction and determined by the target shadow silhouette. Thus the target could be considered as an antenna of the silhouette aperture with a negative gain which reduces the field intensity at the reception side.

Summarising this, the shadow contour theorem [16] declares that the shadow radiation in the optical case is completely determined by the size and geometry of the shadow contour.

As was stressed in [26] the RCS of a complex shape target can be analysed by decomposing it into a number of basic shapes which, when put together represent a replica of the actual target. This is undoubtedly an approximation as the finer-level interactions between parts will not be taken into account, this is however acceptable for our purposes. For the shadow radiation analysis we can represent the complex shape of a target as a composition of the elementary shapes with rectangular cross-section. Thus we will consider scattering on the target with rectangular cross-section, which is equivalent to the radiation by a rectangular aperture antenna with the phase shifted by $\pi/2$ [22] and fundamentally does not depend on the incident wave. Then we can use the same methods of power budget and signal analysis as for conventional radars, including the concept of target RCS σ_{tg} as a measure of the power, re-radiated by the target in the direction of the observation point at distance R: $\sigma_{\mathrm{tg}} = \lim_{R\to\infty} 4\pi R^2\big(|\boldsymbol{E}_{\mathrm{r}}|^2/|\boldsymbol{E}_{\mathrm{i}}|^2\big)$, where $\boldsymbol{E}_{\mathrm{i}}$ and $\boldsymbol{E}_{\mathrm{r}}$ are incident and target re-radiated electric field intensity, respectively. In far field approximation σ_{tg} in the direction of Rx will be defined by the attitude of the aperture at every moment of motion to the incident transmitted field (Fig. 2) and viewing angles θ, ϕ from the receiver/observation point (Fig. 2*a*).

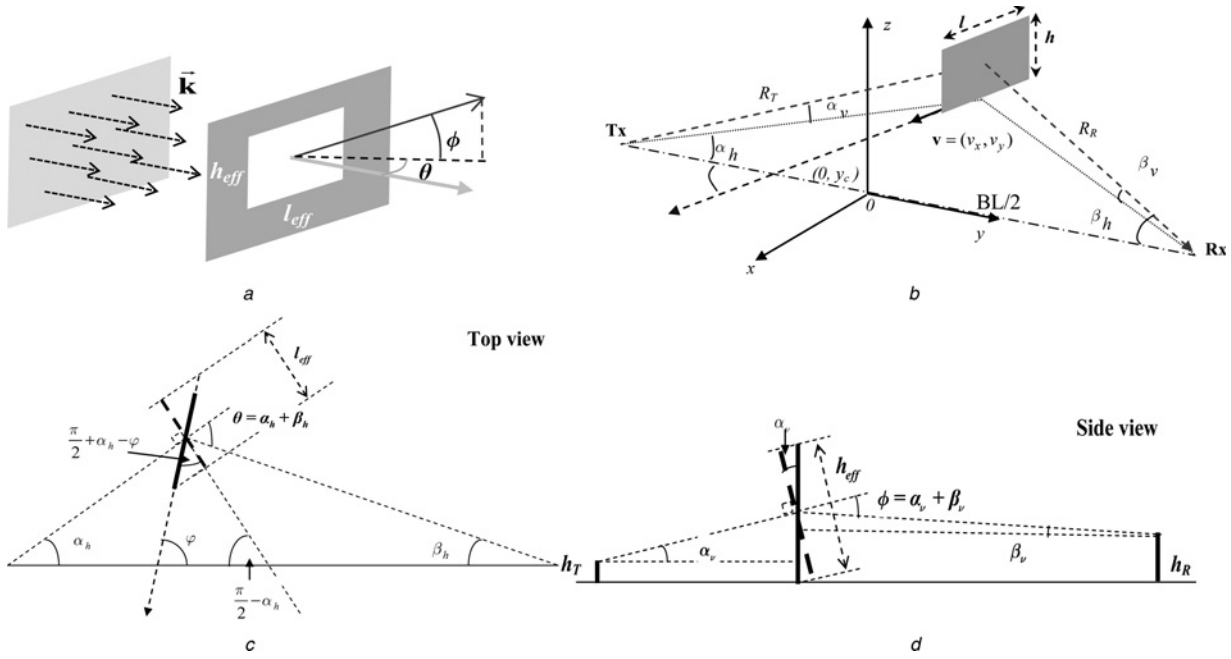

Fig. 2 *Geometries for the calculation of the FS CS of moving target with rectangular cross-section*

a Plane wave incidence on the rectangular plate/aperture and scattering towards observation point (θ, ϕ)
b Bistatic configuration for target moving at the angle φ to the baseline with the speed v
c Top view of rectangular aperture relative to the source and observation point
d Side view of rectangular aperture relative to the source and observation point

For the rectangular aperture the FS CS is [27]

$$\sigma_{\text{fs}}(\theta, \phi) = 4\pi A_{\text{eff}}^2/\lambda^2 \left(\frac{\sin(\pi l_{\text{eff}}/\lambda \sin\theta)}{\pi l_{\text{eff}}/\lambda \sin\theta}\right)^2 \times \left(\frac{\sin(\pi h_{\text{eff}}/\lambda \sin\phi)}{\pi h_{\text{eff}}/\lambda \sin\phi}\right)^2 \tag{10}$$

If rectangular plate moves at a speed $|\boldsymbol{v}|$ and angle φ to the baseline (see notation of Fig. 2*b*) the $\sigma_{\text{fs}}(\theta, \phi)$ is defined by time-varying viewing azimuth and elevation angles $\alpha_h(t)$, $\beta_h(t)$, $\alpha_v(t)$, $\beta_v(t)$, respectively.

Effective aperture area viewed from the Tx (incidence direction) is

$$A_{\text{eff}} = l_{\text{eff}}\ h_{\text{eff}} \tag{11}$$

where l_{eff} and h_{eff} (Figs. 2*c* and *d*) are

$$\begin{aligned} l_{\text{eff}} &= l\cos(\pi/2 + \alpha_h - \varphi) = l\sin(\varphi - \alpha_h) \\ h_{\text{eff}} &= h\cos(\alpha_v) \end{aligned} \tag{12}$$

Viewing angles θ and ϕ from the observation point at Rx are

$$\begin{aligned} \theta &= \alpha_h + \beta_h \\ \phi &= \alpha_v + \beta_v \end{aligned} \tag{13}$$

Thus (10) become

$$\sigma_{\text{fs}}(\theta, \phi, t) = 4\pi \frac{(l\,h)^2 \sin^2(\varphi - \alpha_h)\cos^2(\alpha_v)}{\lambda^2} \times \left(\text{sinc}\left(\frac{\pi l\ \sin(\varphi - \alpha_h)}{\lambda}\sin(\alpha_h + \beta_h)\right)\right)^2 \times \left(\text{sinc}\left(\frac{\pi h\ \cos(\alpha_v)}{\lambda}\sin(\alpha_v + \beta_v)\right)\right)^2 \tag{14}$$

where

$$\begin{aligned} \varphi &= \text{arctg}\left(v_x/v_y\right) \\ \alpha_h(t) &= \text{arctg}\left(\frac{x(t)}{\text{d}T - y(t)}\right), \quad \beta_h(t) = \text{arctg}\left(\frac{x(t)}{\text{d}T + y(t)}\right) \\ \alpha_v(t) &= \text{arctg}\left(\frac{\frac{h}{2} - h_{\text{T}}}{\sqrt{(\text{d}T - y(t))^2 + x^2(t)}}\right), \\ \beta_v(t) &= \text{arctg}\left(\frac{\frac{h}{2} - h_{\text{R}}}{\sqrt{(\text{d}T + y(t))^2 + x^2(t)}}\right) \end{aligned} \tag{15}$$

If the geometrical centre of a rectangular target is exactly on the line between source and receiving point, that is, $\theta = \phi = 0$ ($\alpha_h = \beta_h = 0$, $\alpha_v = \beta_v = 0$) formula (14) reduces to well known

doi: 10.1049/iet-rsn.2012.0233

Table 1 Comparison of simulated and analytical FS CS

φ	Simulated (CST) FS CS dBm^2		Analytical FS CS dBm^2 by (16)	
	f = 5.46 GHz	f = 20 GHz	F = 5.46 GHz	F = 20 GHz
0	−1.79	8.89	−1.99	8.84
15	−2.09	8.56	−2.29	8.54
30	−2.94	7.71	−3.24	7.59
45	−4.85	6.05	−5.00	5.83

expression for the FS CS peak in PO approximation [28]

$$\sigma_{\text{tg}} = \frac{4\pi A_{\text{eff}}^2}{\lambda^2} = \frac{4\pi\left(lh\ \sin(\varphi)\right)^2}{\lambda^2} \tag{16}$$

which indicates 6 dB FS CS rise for twofold increase of frequency.

Simulated in 3D full-wave CST Microwave Studio software and calculated by (16) peaks of FS CS for the rectangular plate 13×9 cm^2 at two frequencies are presented in Table 1 and there is an excellent agreement between them. Such plate has been used for validation of the presented analytical approach and will be discussed in Section 3.

We stress here that in general the independence of the FS CS on the polarisation of the incident wave, stated by PO, is not exactly true for the sub-optical region and, especially, for the Mie scattering regions in case of targets having differing dimensions and finite thickness [27].

Now having both FS CS of extended target by (14) and Doppler phase signature (9) of a point like target the Doppler signature can be presented as

$$S(t) = S_{RO}(t)\,\sigma_{\text{fs}}(t) \tag{17}$$

Doppler signatures with the leakage level (RSSI) of a point-like target and the same but modulated according to FS CS for extended target are shown in Fig. 3.

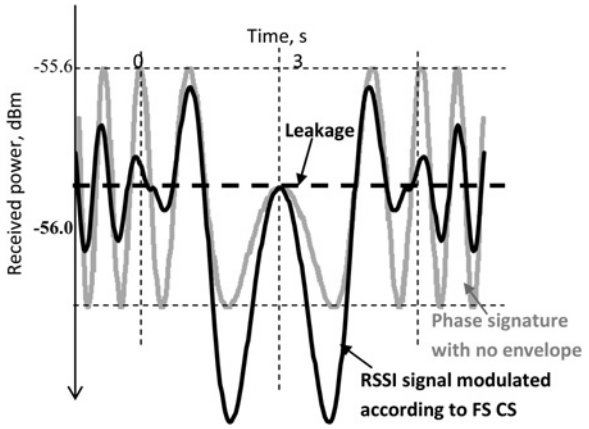

Fig. 3 *Modelled RSSI outputs with and without CS envelope*

3.3 Matched filtering (MF) and speed estimation

The primary objective of optimal signal processing in ground FSR is to maximise signal-to-noise ratio (SNR) by MF. For some particular waveforms at the output of MF, we can observe a signal waveform compression where the autocorrelation function has a narrow main lobe which is much larger than the side lobes. In true FSR for surface targets, the received Doppler waveform is a double-sided chirp signal which after MF will demonstrate such a compression [29, 30].

However for our analysis, the more important output of the MF is extraction of the target motion parameters. It is not within the scope of the paper to consider all aspect of the MF, which can be found in [31], and only briefly the procedure of parameter extraction will be outlined.

The received signal in FSR depends on the target's speed, RCS and trajectory which are unknown a priori. Thus, the optimal filtering process represents the problem of sequential correlation of the received signal with a set of pre-defined reference waveforms $S_{i,j,k}$ covering desired range of velocities and trajectories where i, j, k are indices of $(v_{x,i},\ v_{y,j})|_{i=1..Nx,\ j=1,\ldots,Ny}$ and crossing point $(y_{c,k})|_{k=1,\ldots,K}$ (Fig. 4).

The total number of reference functions in the array is $Nx{\cdot}Ny{\cdot}K$ and is defined by the increments and expected ranges of the parameters under consideration, which in turn are defined by the variety of targets under analysis. Thus the prior knowledge required is in fact the range of speeds and trajectories expected for targets of interest for a specific radar baseline. Obviously, the smaller the increment, the greater the accuracy of the estimated parameters of the target motion. However, in reality the accuracy is specified to be within 1–10% and then the increments can be calculated.

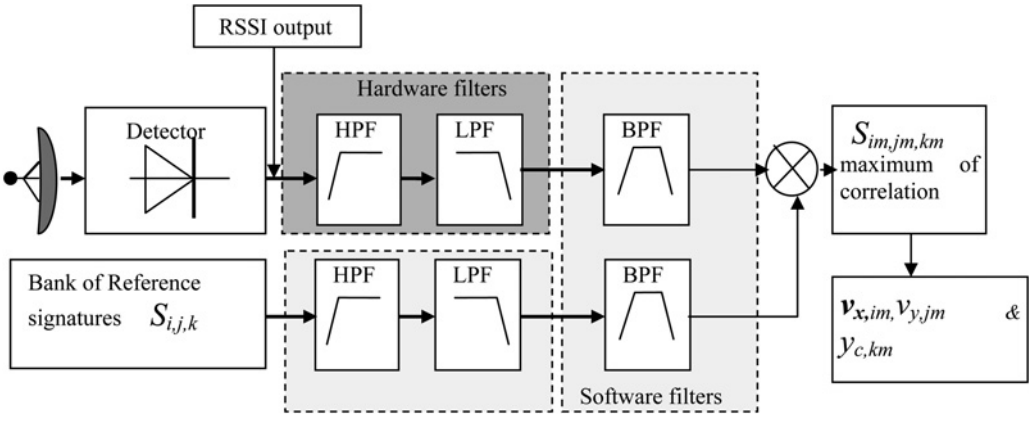

Fig. 4 *Flowchart of the matched filtering procedure*

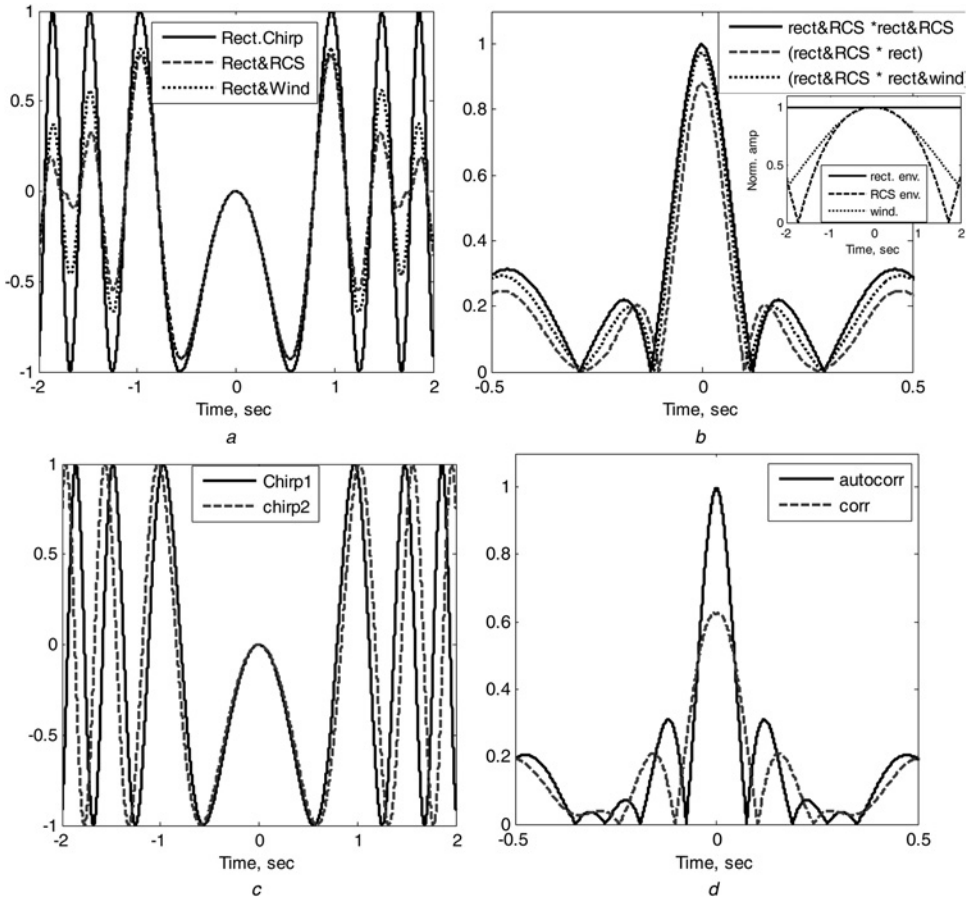

Fig. 5 *Demonstration of the influence of the signal waveform on the resulting convolution with the reference function*

a Rectangular waveforms with different envelopes
c Rectangular waveforms with different chirp frequencies
b and *d* Corresponding compressed signals (correlations)
Inset in panel (*b*) shows different envelopes

According to (9) the generalised form of the reference function is

$$S_{\text{ref}}(t) = -A(t)\sin\left(\frac{2\pi\left(R_{\text{T}}(t) + R_{\text{R}}(t) - L\right)}{\lambda}\right) \qquad (18)$$

where a priory unknown target trajectory and speed are parameters in $R_{\text{T}}(t)$, $R_{\text{R}}(t)$ and $A(t)$.

Although the first two quantities can be modelled within the reasonably small range of expected target motion parameters for a given radar topology, target velocity and crossing point, the amplitude modulation for an arbitrary (unknown) target however could result in a nearly infinite number of pre-defined FSCSs and yet, its effect on MF will be significantly less than that of the $R_{\text{T}}(t)$, $R_{\text{R}}(t)$ terms, which define the argument (phase) of the sinusoid waveform.

In reality the propagation path loss also contributes to the signal modulation because of the attenuation of the signal with the distance. It was shown in [5] that an inverse fourth power law (two-ray path) fits the observation quite well for the ground targets. Therefore ideally in the MF, the reference functions should be modulated in accordance to both RCS (or FS CS-σ) and attenuation. However, propagation path attenuation during observable target motion for the Mie and optical scattering regions is much smaller in comparison to the modulation by the target RCS. As the latter cannot be known in advance, we can only use windowing of the rectangular reference waveform as an appropriate approximation of the RCS envelope within the relatively short integration time. Thus, we assume the actual presence of the envelope expressed by (14) does not affect the estimation of the trajectory when only using the restricted model with the windowed rectangular envelope in (9).

This conclusion is supported by the following reasoning, the chirp like signal is a sign-alternating function. Analysis of the convolution of such a function with itself, but modulated by a more slowly alternating function or, in other words, not having rectangular envelop, shows that such a modulation contributes much less in the result of convolution than any discrepancy between the sign-alternating 'carrier' waveforms being correlated.

Table 2 Relationship between enveloped waveforms and the correlation coefficients between them

	Rectangular chirp	(Rectangular chirp)·RCS	(Rectangular chirp)·(Kaiser window)
norm. power, dB	−3.5081	−6.9014	−6.1426
correlation coeff.	–	1	–
	0.88—		–
	–	0.97—	

doi: 10.1049/iet-rsn.2012.0233

Demonstration of the effect is shown in Fig. 5 and Table 2.

In Fig. 5*a* the modulation according to specific RCS or by Kaiser window (shape factor 2.5) results in about 45% amplitude decrease.

However, correlation coefficient 1 corresponding to autocorrelation of the rectangular waveform modulated according to RCS (here and after – total signal) reduced only to 0.8836 (Table 2) for the convolution of the total signal with the rectangular chirp and to 0.9742 for the convolution of the total signal with the windowed rectangular chirp.

In contrast, change of the chirp frequency only by 10% results in dramatic reduction of the correlation coefficient. In Fig 5*c* the frequency of the chirp 2 is 0.9 of frequency of the chirp 1 – (10% shift) and correlation coefficient drops to 0.63 (Fig. 5*b*).

According to this we will use reference functions as in (9) with only amplitude modulation by windowing rectangular waveform for matched filter and correlate them with the measured signal, which ideally should coincide with the total signal as in (17) (except negligible modulation according to the propagation loss).

More detailed analysis of matched filter performance for FSR could be found in [30].

Thus such MF will demonstrate nearly optimal performance and provides both the improvement of the detection performance as it maximises the SNR and high accuracy of extracted target motion parameters.

4 Model verification in a controllable environment

4.1 Experimental study in anechoic chamber

The main purpose of the measurements was to confirm the approach used for signature modelling. Independency of shadow radiation from the actual target shape and cover has also been investigated by comparison between absorbing and metallic target signatures allowing distinction between forward scatter and bistatic reflections. Two sorts of targets have been used: metallic cylinder (MC) and plate of the same rectangular cross-section $9 \times 13\ \text{cm}^2$ and similar cylinder and plate covered by magnetic absorbing material (RFSB 1062 [32]) with peak of absorption at 5.46 GHz (5.5 cm wavelength).

The geometry of the bistatic configuration is shown in Fig. 6. More details about experiment can be found in [33].

Tx and Rx were positioned at distance $BL = 4.25$ m to provide far field operation. For comparison similar records have been made in monostatic configuration where Tx and Rx antennas were spaced only to give a reasonable isolation.

For 5.5 cm wavelength the scattering from the chosen targets cannot be attributed to purely optical or purely Mie scattering, being rather a boundary case, however as it was

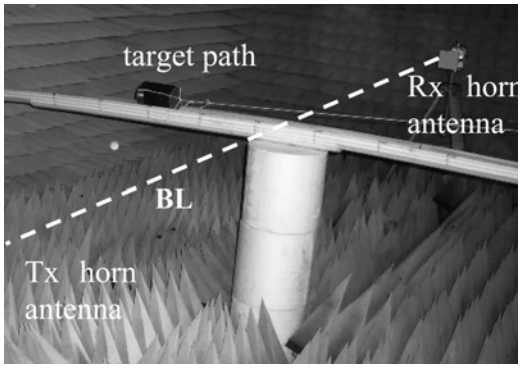

Fig. 6 *Outline of measurement set-up*

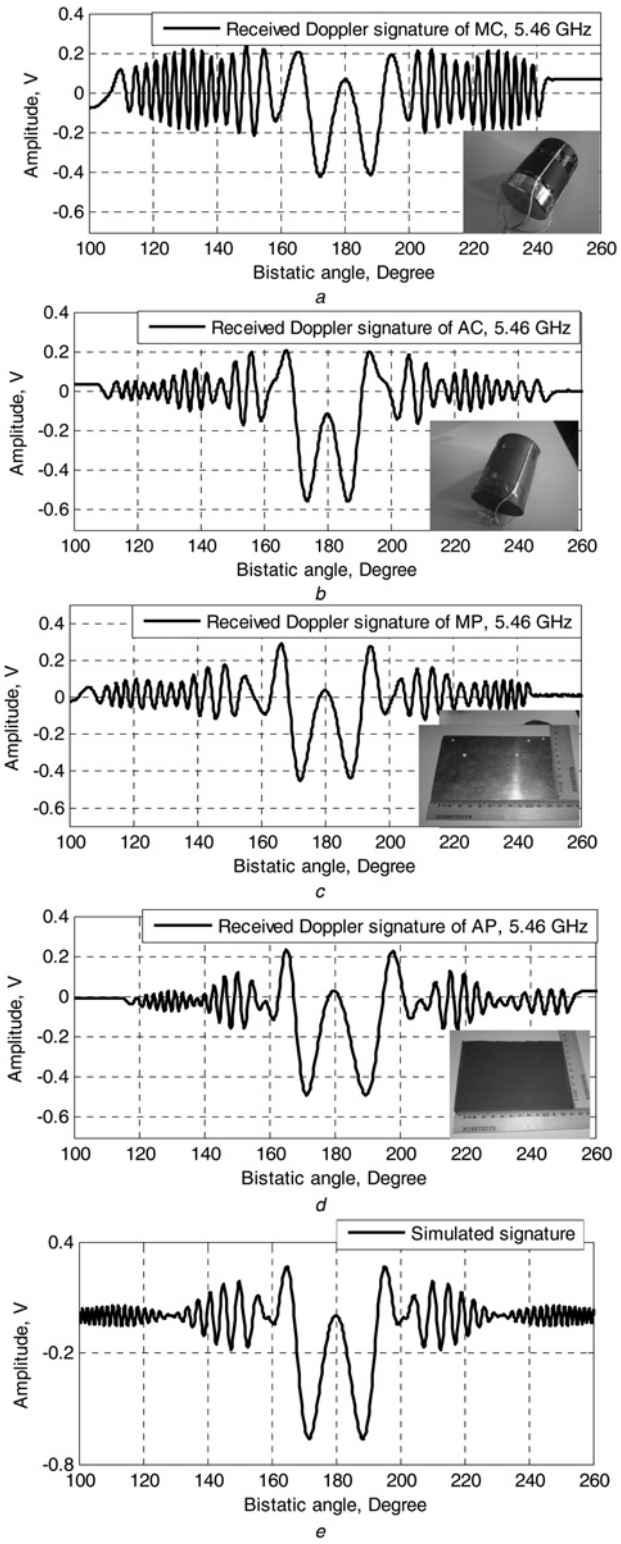

Fig. 7 *Comparison of the measured Doppler signatures of*

a Metallic cylinder
b Absorbing cylinder
c Metallic plate
d Absorbing plate
e Simulated signature of absorbing plate

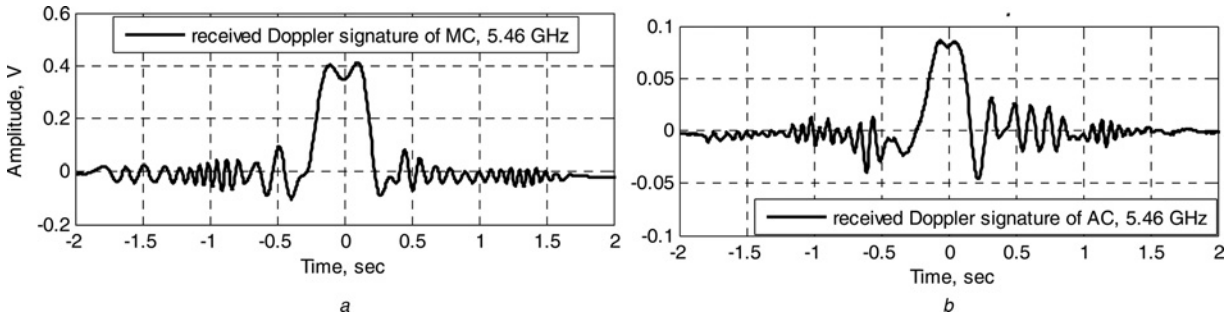

Fig. 8 *Monostatic Doppler signatures of cylinders*

a Metallic
b Absorbing

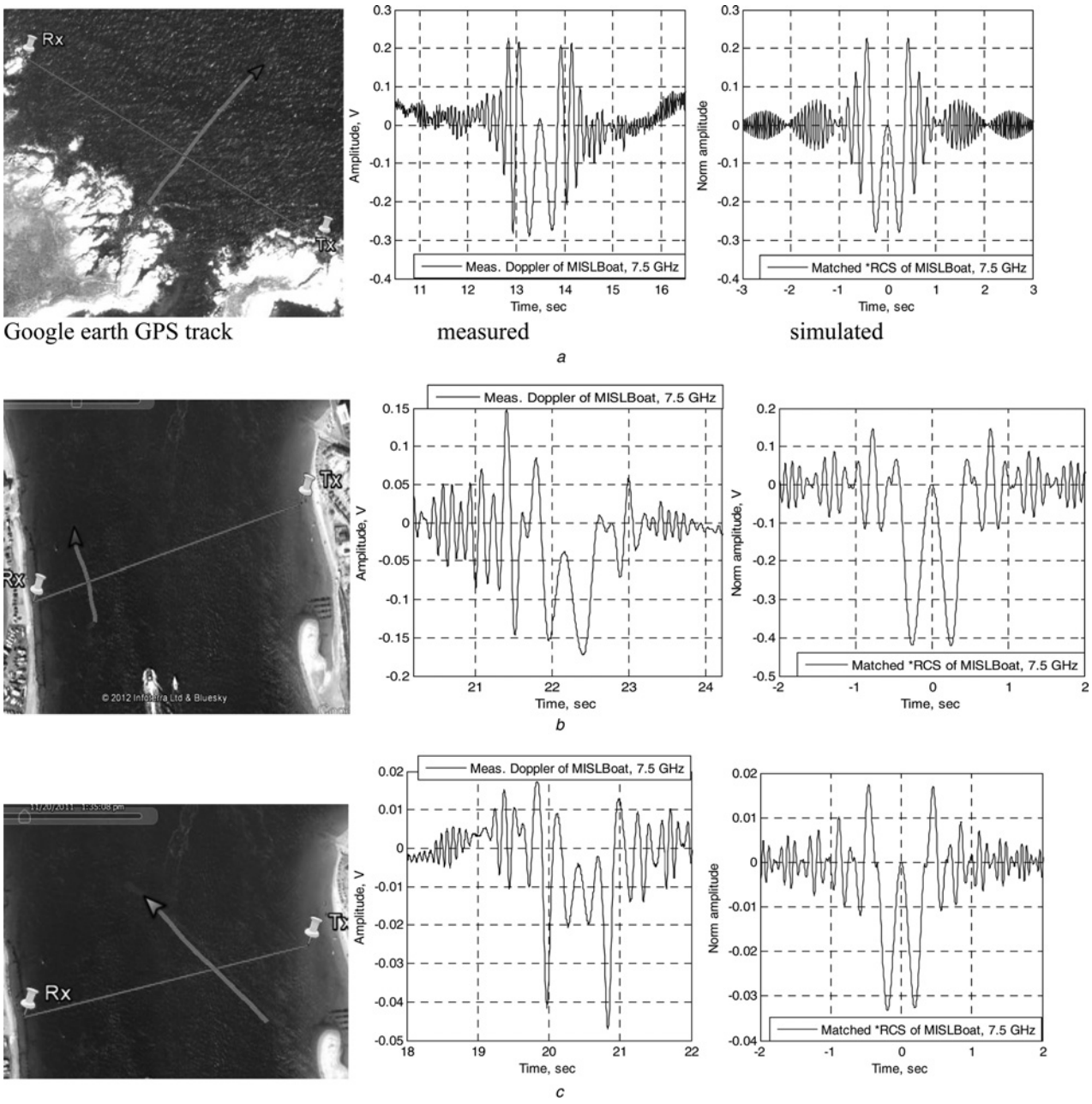

Fig. 9 *Comparison of measured signal with matched signal from coherent processing*

a Middle perpendicular baseline crossing
b Perpendicular baseline crossing closer to Rx
c Crossing at 60° to the baseline
In *a*, *b* and *c*, the left image GPS location and trajectory, middle image, the measured signal, and right image shows the matching signature selected by coherent processing modulated according to the simulated CS of a boat with speed and trajectory parameters defined by MF

doi: 10.1049/iet-rsn.2012.0233

Table 3 Measured (GPS tracking) and extracted parameters (coherent processing) of targets in Fig. 9

	Baseline, m		Speed, v	Crossing angle φ,°	Crossing point, distance from the middle, m
(a)	350 (Bulgaria)	GPS recorded	10–10.3 knots (18.52–19.0756 km/h)	~90	12
		extracted	19.08 km/h	90.0	20.0
(b)	285 (UK)	GPS recorded	6.6–7 knots (12.2232–12.964 km/h)	~90	85.5
		extracted	13.32 km/h	90.0	80.0
(c)	262 (UK)	GPS recorded	9–10.3 knots (16.668–19.0756) km/h	~60	40
		extracted	17.64 km/h	60.0	60.0

shown (Table 1) their FS CS can be estimated as that of a rectangular plate.

Recorded Doppler signatures (RSSI signals with leakage subtracted) are shown in Fig. 7.

The following observations support the above analysis:

1. The envelopes of all signatures in the bistatic range 120–240° coincide reasonably well confirming the validity of approximation of the CS of bodies having rectangular cross-section by the rectangular aperture.
2. Amplitude in the middle part of the signal when the target is crossing the baseline does not depend on the material of the target but the size. This observation completely agrees with the shadow contour theorem for the FS mechanism. Strictly speaking this would not necessarily be true for targets, which are neither perfectly reflective nor represent a black body; however, the deviation will not be significant or noticeable in any practical radar.
3. The amplitude of the signal from the absorbing cylinder decreases gradually as bistatic angles decrease from 150° (larger than 230°) while for the MC the amplitude remains fairly constant within 80°–150° (Figs. 7*a* and *b*). Such behaviour indicates transition from FS to bistatic reflection which explains the smaller amount of the reflected field because of the absorbing cover. Indeed according to [10] the equivalent currents on the illuminated side of the scattering object depend on the anisotropic reflection coefficient $\Re$ resulting in the reflected field components dependency on the reflection coefficient, whereas for the shadow field its components are still exactly the same as for the case of perfectly conducting objects.
4. In all signatures, there is a phase discontinuity observable at about 160° which indicate transition between main and side shadow lobes.

For comparison the dramatic reduction of the amplitude of the backscattering reflection for absorbing cover in a 'monostatic' configuration is shown in Fig. 8. As expected there are two main differences against the FS configuration:

1. Amplitude of the signal is increasing when the aspect angle is about 90°, because a large part of the transmitted energy is reflected backwards resulting in 'positive interference' with the leakage signal in the RSSI channel.
2. Power of the received signals differs between conductive and absorber coated cylinders by about 20 dB. Modelled waveforms as the reference function in coherent processing.

Now we can compare the measured signature with simulation by the described approach. Calculation by (17) requires the knowledge of trajectory and speed ($\boldsymbol{v}$ and φ) of a target which were obtained by MF procedure, outlined in 1.2.

For all records the motion parameters estimated by MF coincide pretty well (within 5% of accuracy) with data truth provided by video records.

Examples of the measured and simulated signatures of absorber covered plate are shown in Figs. 7*d* and *e*. Estimated speed and crossing angle are 1.09 m/s and 90°, accordingly, whereas recorded actual speed is about 1.03 m/s.

The accuracy of simulated signals with respect to measured ones is subject of motion stability. The actual motion is never precisely uniform within the finite time. However, optimal processing will automatically find the reference function that is maximally close to the most representative in terms of energy of the signal in the middle part of the chirp signal and therefore the estimated parameters of motion could be also considered as the most representative for the motion pattern under detection.

5 FSR model validation in real environment

Measurement of small marine targets in real sea conditions have also been undertaken to provide a wide range of trajectories and speeds and to estimate MF algorithm performance with the background sea clutter. Doppler signatures at 7.5 GHz frequency (CW) of a small inflatable boat crossing a baseline of nominal length of 300 m, with different trajectories, at sea state 1–2 near Portsmouth, UK and near St. Ivan Island, Bulgaria were recorded and processed in order to extract the boat motion parameters. Data truth has been provided by a GPS tracking device. Directional Tx/Rx antennas have been used. The boat length is ~2.9 m, its aft (engine compartment) is deeply sinking into the water and nose is protruding by about 1 m above the sea surface when in fast motion. Increments of speed, crossing angle and crossing point for MF were chosen: 0.36 km/h, 15° and 20 m, respectively. Three representative examples are shown in Fig. 9 and results are summarised in Table 3 for: (a) middle perpendicular crossing, (b) crossing closer to Rx and (c) crossing at 60°. The measured signal is shown alongside the matching signature determined by coherent processing and modulated according to the simulated CS of a boat moving at speed and trajectory parameters defined by MF. Discrepancies between recorded and simulated waveforms could be attributed to deviation of the boat motion from being uniform and linear. Indeed strong tidal waves in cases 2 and 3 influenced the uniformity and linearity of motion – in Portsmouth the boat was jumping on the waves with alternating full exposure of the engine and deep immersion

into the water, which may cause fluctuation of RCS of the target. In other words, the boat had a vertical component of the velocity. However, at this stage we cannot give a proven explanation and hope to obtain answers in the next stage of our research on maritime target detection. It was shown in [34] that FS clutter at low grazing angles has a narrow spectrum limited by 1–2 Hz invariant to operational frequency, baseline length and even sea state. Therefore it could be effectively filtered out; however, here we deliberately have shown and processed the raw signals. Even then results of parameter extraction as well as visual waveform analysis confirm excellent agreement between data and ultimately the ability of the suggested approach for modelling, detection and rough recognition.

6 Conclusions

In this paper, the signal formation at the output of FSR Doppler receiver from the target with electrical size defining scattering in the Mie and the optical regions has been analysed.

The main focus has been made on a true forward scatter mode where the surface target actually crosses the radar baseline and FS effect is observed. Using the PO assumptions the equations for target signature modelling have been derived in a traditional for radar engineers' format. These equations have been verified experimentally using calibrated targets with conductive and absorbing coating in a controlled environment and maritime targets in the real sea conditions. In all cases $\pi/2$ phase shift of a shadow signal with respect to the transmitted signal predicted by the PO has been observed. For calibrated targets the transition from shadow to reflective scattering mechanisms has been demonstrated.

It has also been shown that target signature may be represented as a Doppler signature of a point-like target specified by the targets trajectory and speed which is modulated according to FS CS of an actual extended target specified by its silhouette at each moment of motion.

Presented analysis is important for both understanding the physics behind FSR operation and practical system design: estimation of system performance, optimisation of parameters and optimal signal processing algorithms development.

7 References

1 Rohling, H.: '100 years of radar' (Bonn, 2004)
2 Glaser, J.: 'Forward scatter radar for future systems', *WSTIAC Q.*, 2011, **10**, (3), pp. 3–8
3 Willis, N.J., Griffiths, H.D.: 'Advances in bistatic radar' (SciTech Publishing, 2007)
4 Willis, N.: 'Bistatic radar' (SciTech Publishing, 2007)
5 Sizov, V, Cherniakov, M., Antoniou, M.: 'Forward scattering radar power budget analysis for ground targets', *IET Radar Sonar Navig.*, 2007, **1**, (6), pp. 437–446
6 Cherniakov, M., Sizov, V., Myakinkov, A.V.: 'Easily deployable, multi-functional radar network', Proc. Fifth EMRS DTC Tech. Conf., Edinburgh, UK, 2008, pp. 34–37
7 Cherniakov, M., Gashinova, M., Cheng, Hu., Antoniou, M., Sizov, V., Daniel, L.Y.: 'Ultra wideband forward scattering radar: concept and prospective'. Proc. IET Int. Conf. Radar Systems, Edinburgh, UK, October 2007, pp. 1–5
8 Griffiths, H.D., Baker, C.J.: 'Passive coherent location radar systems. Part 1: performance prediction', *IET Radar Sonar Navig.*, 2005, **152**, (3), pp 153–159
9 Griffiths, H.D., Baker, C.J., Ghaleb, H., Ramakrishnan, R., Willman, E.: 'Measurement and analysis of ambiguity functions of off-air signals for passive coherent location', *Electron. Lett.*, 2003, **39**, (13), pp. 1005–1007
10 Ufimtsev, P.: 'New insight into the classical Macdonald physical optics approximation', *IEEE Antennas Propag. Mag.*, 2008, **50**, (3), pp. 11–20
11 Glaser, J.I.: 'Bistatic RCS of complex objects near forward scatter', *IEEE Trans. Aerosp. Electron. Syst.*, 1985, **AES-21**, (1), pp. 70–78
12 Daniel, L., Gashinova, M., Cherniakov, M.: 'Maritime target cross section estimation for an UWB FSR network'. Proc. EuRAD, Amsterdam, Netherlands, October 2008, pp. 316–320
13 Mie, G.: 'Beiträge zur Optik trüber Medien, speziell kolloidaler Metallösungen', *Ann. Phys.*, 1908, **330**, pp. 377–445
14 van de, H.H.C.: 'Light scattering by small particles' (Wiley, New York, 1957)
15 Born, M., Wolf, E.: 'Principles of optics' (Pergamon Press Ltd, London, 1959)
16 Ufimtsev, P.Ya.: 'Fundamentals of the physical theory of diffraction' (John Wiley & Sons, 2007)
17 Gould, D.M., Orton, R.S., Pollard, R.J.E.: 'Forward scatter radar detection'. Proc. RADAR 2002 Conf., Edinburgh, UK, 15–17 October 2002, pp. 36–40
18 Jackson, J. D.: 'Classical electrodynamics', (John Wiley & Sons, 1999)
19 Hiatt, R.E., Siegel, K.M., Weil, H.: 'Forward scattering by coated objects illuminated by short wavelength radar', *Proc. IRE*, 1960, **48**, (9), pp. 1630–1635
20 Skolnik, M.I., 'Radar handbook' (McGraw-Hill, 1989, 2nd edn.)
21 Cherniakov, M., Abdullah, R.S.A.R., Jancovic, P., Salous, M., Chapursky, V.: 'Automatic ground target classification using forward scattering radar', *IEE Proc. Radar Sonar Navig.*, 2006, **153**, (5), pp. 427–437
22 Ross, R.A.: 'Forward scattering from a finite, circular cylinder', *Prog. Electromagn. Res. C*, (2), 2008, pp. 207–215
23 Ruck, G.T., Barrick, D.E., Stuart, K.M., Kirchbaum, C.K.: 'Radar cross section handbook' (Plenum Press, NY, 1970, vol. 1)
24 http://www.cst.com/Content/Documents/Events/Downloads/Event_item_1731/CST_Installed_performance.pdf, accessed August 2012
25 Rashid, N.E.A., Antoniou, M., Jancovic, P., Sizov, V., Abdullah, R., Cherniakov, M.: 'Automatic target classification in a low frequency FSR network'. Proc. EuRAD, Amsterdam, Netherlands, October 2008, pp. 68–71
26 Balanis, C.A.: 'Antenna theory' (John Wiley and Sons, 2005)
27 Balanis, C.A.: 'Advanced engineering electromagnetics' (John Wiley & Sons, 1989)
28 Seigel, K. M.: 'Bistatic radars and forward scattering', Proc. National Conf. Aeronautical Electronics, Dayton, Ohio, US, 12–14 May 1958, pp. 286–290
29 Hu, C., Antoniou, M., Sizov, V., Cherniakov, M.: 'Quasi-optimal signal processing in ground forward scattering radar', Proc. IEEE Radar Conf., Rome, Italy, May 2008, pp. 1–6
30 Cheng Hu, Sizov V., Antoniou M., Gashinova M., Cherniakov, M.: 'Optimal signal processing in ground-based forward scatter micro radars', *IEEE Trans. Aerospace Electr. Syst.*, 2012, **48**, (4), pp. 3006–3026
31 Levin, B.R.: 'Theoretical principles of statistical radiophysics [in Russian]' (Sovetskoe. Radio, Moscow, 1969)
32 http://www.lairdtech.com, accessed August 2012
33 Gashinova, M., Daniel, L., Kabakchiev, K., Sizov, V., Hoare, E., Cherniakov, M.: 'Phenomenology of signals in FSR for surface targets detection', Int. Conf. Radar Systems RADAR 2012, Glasgow, UK, 22–25 October 2012
34 Hoare, E.G., Daniel, L.Y., Gashinova, M., *et al.*: 'Near zero grazing angle forward scatter sea clutter spectrum analysis', IET Int. Conf. Radar Systems, Glasgow, October 2012

doi: 10.1049/iet-rsn.2012.0233